

Synchronization of pairwise-coupled, identical, relaxation oscillators based on metal-insulator phase transition devices: A Model Study

Abhinav Parihar,^{1, a)} Nikhil Shukla,^{2, b)} Suman Datta,^{2, c)} and Arijit Raychowdhury^{1, d)}

¹⁾*School of Electrical and Computer Engineering, Georgia Institute of Technology, Atlanta, Georgia 30332, USA*

²⁾*Department of Electrical Engineering, Pennsylvania State University, University Park, Pennsylvania 16802, USA*

Computing with networks of synchronous oscillators has attracted wide-spread attention as novel materials and device topologies have enabled realization of compact, scalable and low-power coupled oscillatory systems. Of particular interest are compact and low-power relaxation oscillators that have been recently demonstrated using MIT (metal-insulator-transition) devices using properties of correlated oxides. Further the computational capability of pairwise coupled relaxation oscillators has also been shown to outperform traditional Boolean digital logic circuits. This paper presents an analysis of the dynamics and synchronization of a system of two such identical coupled relaxation oscillators implemented with MIT devices. We focus on two implementations of the oscillator: (a) a D-D configuration where complementary MIT devices (D) are connected in series to provide oscillations and (b) a D-R configuration where it is composed of a resistor (R) in series with a voltage-triggered state changing MIT device (D). The MIT device acts like a hysteresis resistor with different resistances in the two different states. The synchronization dynamics of such a system has been analyzed with purely charge based coupling using a resistive (R_C) and a capacitive (C_C) element in parallel. It is shown that in a D-D configuration symmetric, identical and capacitively coupled relaxation oscillator system synchronizes to an anti-phase locking state, whereas when coupled resistively the system locks in phase. Further, we demonstrate that for certain range of values of R_C and C_C , a bistable system is possible which can have potential applications in associative computing. In D-R configuration, we demonstrate the existence of rich dynamics including non-monotonic flows and complex phase relationship governed by the ratios of the coupling impedance. Finally, the developed theoretical formulations have been shown to explain experimentally measured waveforms of such pairwise coupled relaxation oscillators.

Keywords: Relaxation oscillators, coupling, anti-phase locking, in-phase locking, bistable systems, phase locking and synchronization

With insurmountable challenges facing silicon scaling, research has started in earnest to identify potential computational architectures and device technologies for a post-silicon era. One such paradigm where coupled oscillatory systems perform computational tasks such as pattern recognition and template matching has garnered recent interest; and it necessitates the fabrication of compact and scalable oscillators that can be electrically coupled. Recent advances in the development of correlated oxides have led to successful demonstration of coupled relaxation oscillators. Here we investigate the coupling dynamics of pairwise coupled identical relaxation oscillators based on such correlated materials that exhibit electrically controlled metal-insulator-metal phase transitions. Using analytical and numerical techniques we show how the coupling network can lead to in-phase and out-of-phase locking as well as create a bistable system. Such systems have already been shown to offer computational capabilities beyond the traditional Boolean fabric.

I. Introduction

Synchronization of systems of oscillators has attracted widespread attention among physicists, mathematicians and neurobiologists alike. Even simple descriptions of oscillators and their coupling mechanisms give rise to rich dynamics. Synchronization dynamics of coupled oscillators not only have a wide variety of applications in engineering^{1,2} but they also explain many natural, chemical and biological synchronization phenomena like the synchronized flashing of fireflies, pacemaker cells in the human heart, chemical oscillations, neural oscillations, and laser arrays, to name a few³. Coupled sinusoidal oscillators have been extensively studied^{4,5,6} and their application in the computational paradigm has been well demonstrated^{7,8}. A generalized description of oscillators in these models is usually a canonical phase model^{3,9}, and the coupling mechanisms is generally assumed weak and composed of simple periodic functions. Several studies on more general periodic coupling functions have been studied¹⁰. Along with sinusoidal oscillators, non-linear Van-der-Pol oscillators and several of its variants have also been studied and the applicability of such models in neurobiological and chemical oscillators have been demonstrated¹¹⁻¹⁴. Such analytic models of coupled oscillatory systems almost always require a canonical phase description of the oscillators and a periodic phase dependent additive coupling that can be classified as weak. Although such a description of a system of oscillators is elegant and provide key insights, relaxation oscillators

^{a)}Electronic mail: aparihar6@gatech.edu

^{b)}Electronic mail: nss152@psu.edu

^{c)}Electronic mail: sdatta@enr.psu.edu

^{d)}Electronic mail: arijit.raychowdhury@ece.gatech.edu

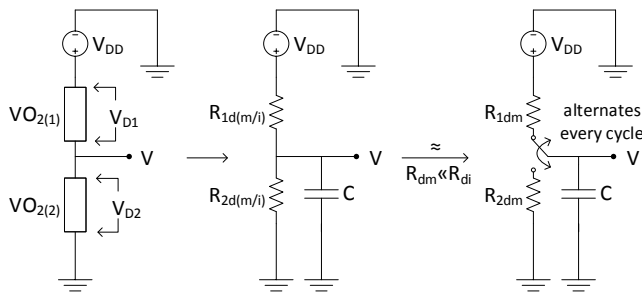


Figure 1: Relaxation oscillator circuit realized using two MIT state-changing devices in series (D-D configuration), and its circuit equivalent with R_{dm} and R_{di} as the internal resistance of the MIT devices in metallic and insulating states respectively. When $R_{di} \gg R_{dm}$ the device behaves as a parallel combination of a capacitor and a resistor with a switch.

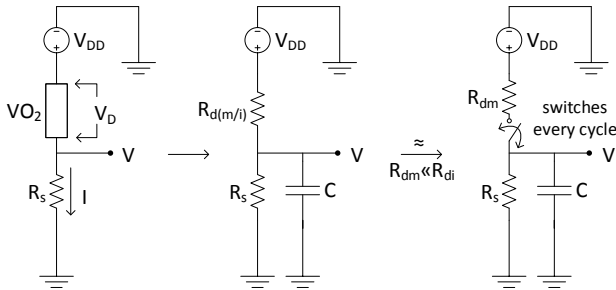


Figure 2: Relaxation oscillator circuit realized with a MIT device in series with a resistor (D-R configuration), and its circuit equivalent with R_{dm} and R_{di} as the internal resistance of the MIT device in metallic and insulating states respectively. When $R_{di} \gg R_{dm}$ the device behaves as a parallel combination of a capacitor and a resistor with a switch.

that have recently been demonstrated using phase transition MIT devices, cannot be modeled using such a simple phase description. Prior work by the authors have experimentally demonstrated locking and synchronization in a pairwise coupled system of relaxation oscillators² and its possible application in computation has also been discussed¹. The coupling behavior of relaxation oscillators illustrate complex dynamical properties¹⁵ and in this paper we study the synchronization behavior of a pair of identical and electrically coupled relaxation oscillators². Individual oscillators are composed of either two MIT devices in series (D-D configuration) or a MIT device in series with a linear resistor (D-R configuration)² and electrical coupling is enabled through a parallel connected R-C network. We show, through analytical and numerical techniques how the final steady state relative phase of such coupled oscillators depend on the coupling function. For certain range of values of the coupling function, we note the possibility of a bistable system, where both in-phase and out-of-phase locking are stable, thereby giving rise to the possibility of using such oscillatory networks in computation^{1,8}.

II. Electrical Circuit Model and Representation

An electrical circuit representation of the relaxation oscillators is important to define the form of coupling which is physically realizable. The basic relaxation oscillator involves repeated charging and discharging of a capacitor through a resistive path. Switching between charging and discharging has to be done autonomously by the circuit configuration. In

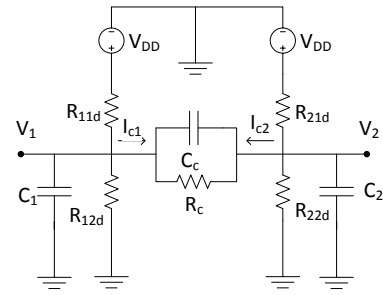


Figure 3: Circuit equivalent of coupled D-D oscillators with an RC circuit used as the coupling circuit. For D-R oscillators, one state-changing resistor of each oscillator is replaced by a constant linear resistor

this paper, we are concerned with the relaxation oscillators built using state-changing devices. Such state-changing devices are fabricated using correlated oxide (vanadium dioxide, VO_2) and exhibit MIT (metal-insulator transition) where the device switches between a metallic and an insulating state under the application of heat or an electric field¹⁶. Further details about the physical implementation of these devices are discussed in section VIII. We will consider two kinds of relaxation oscillator circuits using such state-changing devices - (a) two state-changing devices in series (figure 1). We will refer to this configuration as D-D. And (b) a state changing device in series with a resistance (figure 2)². This configuration will be referred to as D-R. The D-D configuration is enticing in its simplicity, both in physical realization and analysis as will be evident in the following sections. The D-R configuration, on the other hand, has already been experimentally demonstrated² and can be thought of as an extension of the D-D configuration albeit with more complex dynamics of synchronization. In this paper we will first study the D-D configuration, using analytical and numerical techniques; and show through phase models and flow analysis some key results in the D-R configuration.

The state transition of the device follow:

- Only the resistance of the device changes with its state; and the resistance is linear;
- A state transition is triggered by the voltage across the device. This triggering can be electric field driven or thermally driven, and can be modeled as an equivalent triggering voltage². When the voltage exceeds a higher threshold v_h , the state changes to a metallic (low resistance) state and when the voltage exceeds a lower threshold v_l , the state switches back to the insulating (high resistance) state. The thresholds v_h and v_l are not equal, i.e. there is hysteresis in the switching with $v_l < v_h$, and
- A capacitance is associated with the device that ensures gradual build up and decaying of the voltage (and hence energy) across the device v_D .

The present study of the synchronization dynamics of such coupled systems, although inspired by the experimental realization of VO_2 based oscillators, is not limited to these oscillators only, but encompasses a class of similar pairwise-coupled relaxation oscillators as well. The circuit equivalents of single and coupled relaxation oscillators are shown in figure 1,

figure 2 and figure 3 respectively. The internal resistance of the device R_d has two different values in the two states of the device - R_{di} in the insulating (high resistance) state and R_{dm} in the metallic (low resistance) state. C is the internal capacitance of the MIT device (including any parasitic capacitances) and R_S is the series resistance. We will also assume that $R_{di} \gg R_{dm}$. In the D-D configuration, the capacitor being charged can be represented as a single capacitor at the output circuit node. The coupling circuit is a parallel combination of a capacitor C_c and a resistor R_c . As shown, the output node of the oscillator is between the device and the resistance, and the coupling circuit is connected between these output nodes².

III. Model Development For Isolated & Coupled Oscillators

Before investigating the system dynamics, let us establish the system model and the system of ODEs that define the system. This will allow us to define the conditions for oscillation as well as the coupling dynamics. We will first consider D-D configuration and then D-R configuration as an extension of the D-D configuration. The D-D configuration, owing to its inherent symmetry renders to easier dynamics and analysis and provides valuable insights into the system. Such key numerical and analytical results for this are discussed in the following sections.

A. D-D configuration

The circuit equivalent for a D-D type relaxation oscillator is shown in figure 1. For simplicity, all voltages are normalized to v_{dd} (including v_l and v_h). We define conductances $g_{di} = R_{di}^{-1}$, $g_{dm} = R_{dm}^{-1}$ and $g_c = R_C^{-1}$. For the conductances, subscript d denotes a state dependent device conductance and m/i denotes metallic/insulating state respectively. The subscripts preceding dm or di refer to the corresponding numbered device as shown in figure. Also, it is assumed that $g_{dm} \gg g_{di}$, which means that the g_{di} state essentially disconnects the circuit. This implies that the effective charging happens through g_{1dm} and effective discharging through g_{2dm} . The single D-D oscillator can be described by the following set of piecewise linear differential equations:

$$cv' = \begin{cases} (v_{dd} - v)g_{1dm} & \text{charging} \\ -vg_{2dm} & \text{discharging} \end{cases} \quad (1)$$

where c is the lumped capacitance of both devices along with the parasitics. The equation can be re-written as:

$$cv' = -g(s)v + p(s) \quad (2)$$

where s denotes the conduction state of the device (0 for metallic, and 1 for insulating) and $g(s)$ and $p(s)$ depend on the device conduction state s as follows:

$$g(s) = \begin{cases} g_{1dm}, & s = 0 \\ g_{2dm}, & s = 1 \end{cases} \quad (3)$$

$$p(s) = \begin{cases} g_{1dm}, & s = 0 \\ 0, & s = 1 \end{cases} \quad (4)$$

When two identical oscillators are coupled in a manner described in figure 3, the system can be described by the follow-

ing coupled equations:

$$c_1 v_1' = \begin{cases} (v_{dd} - v_1)g_{11dm} - i_{c1} & \text{charging} \\ -v_1 g_{12dm} - i_{c1} & \text{discharging} \end{cases} \quad (5)$$

$$c_2 v_2' = \begin{cases} (v_{dd} - v_2)g_{21dm} - i_{c2} & \text{charging} \\ -v_2 g_{22dm} - i_{c2} & \text{discharging} \end{cases} \quad (6)$$

where c_1 and c_2 are the lumped capacitances of the oscillators. For conductances g , the first subscript denotes the oscillator and the second denotes the device. $i_{c1} = -i_{c2}$ is the coupling current given by:

$$i_{c1} = (v_1' - v_2')c_c + (v_1 - v_2)g_c \quad (7)$$

When coupled, the system has 4 conduction states $s = s_1 s_2 \in \{00, 01, 10, 11\}$ corresponding to the 4 combinations of s_1 and s_2 . Analogous to (2), the coupled system can be described in matrix form as:

$$c_c F x'(t) = -g_c A(s)x(t) + P(s) \\ x'(t) = -\frac{g_c}{c_c} F^{-1} A(s) (x(t) - A^{-1}(s)P(s)) \quad (8)$$

where $x(t) = (v_1(t), v_2(t))$ is the state variable at any time instant t . The 2×2 matrices F and $A(s)$, and vector $P(s)$ are given by:

$$F = \begin{bmatrix} 1 + \alpha_1 & -1 \\ -1 & 1 + \alpha_2 \end{bmatrix} \quad (9)$$

$$A(00) = \begin{bmatrix} -\beta_{11} - 1 & 1 \\ 1 & -\beta_{21} - 1 \end{bmatrix}, \quad P(00) = \begin{bmatrix} \beta_{11} \\ \beta_{21} \end{bmatrix} \\ A(10) = \begin{bmatrix} -\beta_{12} - 1 & 1 \\ 1 & -\beta_{21} - 1 \end{bmatrix}, \quad P(10) = \begin{bmatrix} 0 \\ \beta_{21} \end{bmatrix} \\ A(01) = \begin{bmatrix} -\beta_{11} - 1 & 1 \\ 1 & -\beta_{22} - 1 \end{bmatrix}, \quad P(01) = \begin{bmatrix} \beta_{11} \\ 0 \end{bmatrix} \\ A(11) = \begin{bmatrix} -\beta_{12} - 1 & 1 \\ 1 & -\beta_{22} - 1 \end{bmatrix}, \quad P(11) = 0 \quad (10)$$

Here, $\alpha_i = c_i/c_c$ is the ratio of the combined lumped capacitance of i^{th} oscillator to the coupling capacitance c_c , and $\beta_{ij} = g_{ijdm}/g_c$ is the ratio of the metallic state resistance of j^{th} device of i^{th} oscillator, where $i \in \{1, 2\}$ and $j \in \{1, 2\}$. The fixed point in a conduction state s is given by $p_s = A^{-1}(s)P(s)$ and the matrix determining the flow (the *flow matrix* or the *velocity matrix*) is given by $\frac{g_c}{c_c} F^{-1} A(s)$ as can be seen in equation (8). In section V we analyze the steady state locking and synchronization dynamics of two such identical oscillators coupled with a parallel resistive and capacitive element as shown in figure 3.

B. D-R configuration

The equivalent circuit for a D-R type relaxation oscillator is shown in figure 2. As in the case of D-D configuration, voltages are normalized to v_{dd} . The conductances involved are $g_{di} = R_{di}^{-1}$, $g_{dm} = R_{dm}^{-1}$, $g_s = R_s^{-1}$ and $g_c = R_C^{-1}$. Effective charging happens through g_{dm} as in the previous case but there is an added leakage through g_s , whereas effective discharging happens only through g_s . Following the same methodology as in the D-D case, the equation for the single D-D oscillator dynamics can be written as:

$$cv' = \begin{cases} (v_{dd} - v)g_{dm} - v g_s & \text{charging} \\ -v g_s & \text{discharging} \end{cases} \quad (11)$$

which can be re-written as:

$$cv' = -g(s)v + p(s) \quad (12)$$

where,

$$g(s) = \begin{cases} g_{dm} + g_s, & s = 0 \\ g_s, & s = 1 \end{cases} \quad (13)$$

$$p(s) = \begin{cases} g_{dm}, & s = 0 \\ 0, & s = 1 \end{cases} \quad (14)$$

and s denotes the conduction state of the system as before. In case of coupled D-R oscillators, arguments similar to the previous case lead to the same matrix equation as (8):

$$x'(t) = -\frac{g_c}{c_c} F^{-1} A(s) (x(t) - A^{-1}(s)P(s)) \quad (15)$$

where matrices F and P remain the same as before but matrix A changes to the following:

$$F = \begin{bmatrix} 1 + \alpha_1 & -1 \\ -1 & 1 + \alpha_2 \end{bmatrix} \quad (16)$$

$$A(00) = \begin{bmatrix} -\beta_1 - \beta_{s1} - 1 & 1 \\ 1 & -\beta_2 - \beta_{s2} - 1 \end{bmatrix}, \quad P(00) = \begin{bmatrix} \beta_1 \\ \beta_2 \end{bmatrix}$$

$$A(10) = \begin{bmatrix} -\beta_{s1} - 1 & 1 \\ 1 & -\beta_2 - \beta_{s2} - 1 \end{bmatrix}, \quad P(10) = \begin{bmatrix} 0 \\ \beta_2 \end{bmatrix}$$

$$A(01) = \begin{bmatrix} -\beta_1 - \beta_{s1} - 1 & 1 \\ 1 & -\beta_{s2} - 1 \end{bmatrix}, \quad P(01) = \begin{bmatrix} \beta_1 \\ 0 \end{bmatrix}$$

$$A(11) = \begin{bmatrix} -\beta_{s1} - 1 & 1 \\ 1 & -\beta_{s2} - 1 \end{bmatrix}, \quad P(11) = 0 \quad (17)$$

Here $\beta_i = g_{dm}/g_c$ and $\beta_{si} = g_{si}$.

For all numerical simulations in the rest of the paper, the normalized values of v_l and v_h w.r.t v_{dd} are chosen to be 0.2 and 0.8 respectively.

IV. Phase Space, Flows and Oscillation Conditions

A. Single Oscillators

A series arrangement of two MIT devices (D-D), or an MIT device and a resistor (D-R) will oscillate only when certain conditions are met. In case of two devices in series (D-D), the two devices must be in opposite conduction states (one metallic and the other insulating) all the time for oscillations to occur. If the threshold voltages v_l and v_h are same for the devices and the following condition holds

$$v_l + v_h = V_{DD} \quad (18)$$

and at $t = 0$ the devices are in different conduction states, then any time one device switches, the other will make the opposite transition as well. The basic mechanism of oscillations is as follows. The device in metallic state connects the circuit and charges (discharges) the output capacitor, and the other device in insulating state does not participate in the dynamics. As the capacitor charges, the voltage drop across the device in metallic state decreases and crosses the lower threshold v_l . At the same instant, the voltage drop across the other device in insulating state increases and crosses the higher threshold v_h because $v_{D1} + v_{D2} = V_{DD}$. The devices then switch states and the cycle continues. The devices can be conceived as a switch which is open in insulating state (ignoring any leakage in the insulating state) and closed in metallic state (1). If v_l and v_h deviate from (18), the devices will not switch at the

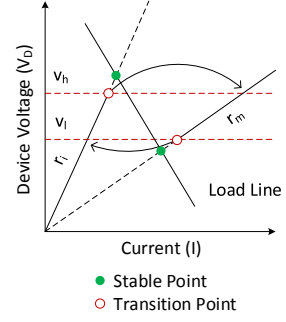


Figure 4: Phase space of the device in a single D-R oscillator. Lines with slopes r_i and r_m are the regions of operation in insulating and metallic conduction states respectively. The intersection of these regions with the load line are the stable points in each region of operation. The transition points should be encountered before reaching the stable points for sustained oscillations as shown

same instant and oscillations will stop as the system settles to a stable point where both devices are in same state and the voltage of the output nodes remains at $V_{DD}/2$. This may require additional startup circuit in the system, which is trivial to integrate.

In D-R configuration, another set of conditions have to be met¹⁷ which depend on the relative values of the device resistances in the two states (R_{dm} and R_{di}) and the series resistance (R_s). These conditions can be described using the phase diagram of the MIT device figure 4. Lines with slopes r_i and r_m are the regions of operation of the device in insulating and metallic states respectively. The intersection of these lines with the load line due to the series resistance gives the stable points of the system in the two states. For self-sustained oscillations, the stable points in each state should lie outside the region of operation, i.e. outside the region defined by horizontal lines passing through the transition points. This ensures that the system always tries to reach the stable point in the current state but is always preceded by a transition to the other state. This moves the system towards the stable point of the other state (away from the previous stable point) and hence the system never reaches any stable point and oscillates. This configuration is robust towards deviation of v_l and v_h from condition (18) and as only one device is involved, it does not require the difficult constraint of simultaneous switching of devices as was in the D-D case. This reduced requirement of symmetry is an attractive property of the D-R configuration as initial experiments have confirmed sustained oscillations in this configuration².

We define the region of operation of a device (and hence of an oscillator) as the region where the device voltage lies between v_l and v_h (or the output voltage lies between $1 - v_l$ and $1 - v_h$). For the D-D case, the oscillators are expected to remain within the region of operation all the time. However in the D-R case, the system can go outside the region of operation in a specific manner as described later.

B. Coupled Oscillators

For analyzing the coupled circuits, the phase diagram of a coupled system can be drawn in the $v_1 \times i_1 \times v_2 \times i_2$ space as was done in figure 4. However, we note that in a given conduc-

tio state of the system, $s = s_1 s_2$, (v_1, v_2) can uniquely identify the system, and hence, $v_1 \times v_2$ space is sufficient for a phase diagram. Therefore, we can draw 4 different phase diagrams of the system for each conduction state s (figure 5) with transitions among them¹⁵ (figure 6). The transitions occur at the edges when either v_1 or v_2 reach the higher or lower threshold for state change from metallic to insulating or vice versa. The flows in each of the 4 conduction states are linear flows and hence have a single fixed point (figure 5). The conditions for oscillations can be described using figure 7. Analogous to the case of a single oscillator, these stable points should lie outside the region of operation (in the shaded region) in a way that the system always tries to move towards these stable points but should be preceded by a state transition which occurs when the system reaches the (red) dashed lines.

1. Monotonic Flows and Periodic Orbits

The conditions of figure 7 are general enough to hold for both D-D and D-R configurations and they ensure that the system does not settle down to a stable point and voltages across oscillators repeatedly increase and decrease. However, these conditions do not ensure the existence of a stable orbit which can give periodic oscillations. To ensure existence of a stable periodic orbit, we consider additional conditions for the systems. For D-D configuration, we consider systems where the flows in the states are monotonic, i.e. v_1 and v_2 are either constantly increasing or constantly decreasing in the region of operation of any conduction state. Figure 6 show these monotonic directions with the state transitions for D-D coupled oscillator configurations. It is proved later that for two identical coupled D-D oscillators, this condition of monotonicity of the flows is *sufficient* for existence of a stable orbit and hence for periodic oscillations. For D-R coupled oscillators, we consider systems where either the direction of flows are strictly monotonic as shown in figure 6 or are non-monotonic in a very specific way as discussed in VII (see figure 23). In this case, periodic oscillations can be ensured for certain conditions as described in section VII. It should be noted here that in the D-R case, the system can also go outside the region of operation as seen in figure 8, but if the fixed points lie in the above mentioned shaded regions, the system will always oscillate. Figure 8 shows typical time-domain waveforms and corresponding phase-space trajectories for the coupled oscillators of the D-D and D-R types.

V. Symmetric D-D coupled oscillator dynamics

Let us first investigate the case when the D-D oscillators are identical and their effective charging and discharging rates are equal, i.e. $\beta_{11} = \beta_{21} = \beta_{12} = \beta_{22} = \beta$ and $\alpha_1 = \alpha_2$. This corresponds to a well designed and ideal oscillator system where the pull-up and pull-down device resistances have been matched to create equal charging and discharging rates. In such a scenario the velocity matrices in the four conduction states $\frac{g_c}{c_c} F^{-1} A(s)$ become equal. As such, the state spaces in the four conduction states can be represented in a common state space with the system flow described by the common velocity matrix and a single fixed point. However, in this common state space, the regions of operation in the four conduction states will be four distinct regions. The position of these

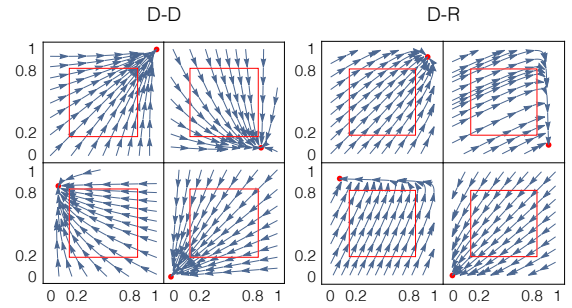


Figure 5: The coupled system can be described by 4 different phase spaces for each state $s = s_1 s_2$. This figure shows the system flows of the D-D and D-R coupled oscillator system in the 4 regions of operation along with the fixed points (shown as red dots) in each state. This figure also represents the simplified case where the flows are monotonic within the region of operation

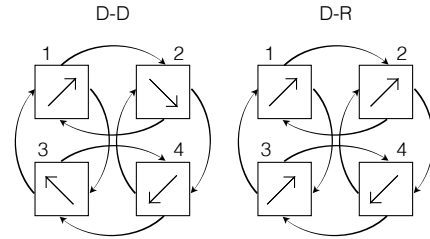


Figure 6: Schematic representation showing the monotonic flow directions in the regions of operation in the simplified model. The monotonicity condition is sufficient for existence of a steady state periodic orbit in the D-D case. Transitions are shown among the 4 states 1(MM), 2(IM), 3(MI) and 4(II) of the coupled system when the system reaches any edge, i.e. the voltage of any oscillator reaches a phase change threshold of its MIT device

regions for a conduction state would depend on the position of its respective fixed points in the original state space. Such a combined phase space is shown in figure 9.

The symmetry of the system is apparent in the flow as well. The eigen values λ_1, λ_2 and eigen vectors e_1, e_2 of the velocity matrix $\frac{g_c}{c_c} F^{-1} A$ of the symmetric system are

$$\lambda_1 = -\frac{g_c}{c_c} \left(\frac{\beta}{\alpha} \right), \lambda_2 = -\frac{g_c}{c_c} \left(\frac{\beta + 2}{\alpha + 2} \right) \quad (19)$$

$$e_1 = \begin{bmatrix} 1 \\ 1 \end{bmatrix}, e_2 = \begin{bmatrix} -1 \\ 1 \end{bmatrix} \quad (20)$$

Real negative eigen values imply that the flow of the system is symmetric about both the eigen vector directions (i.e. a mir-

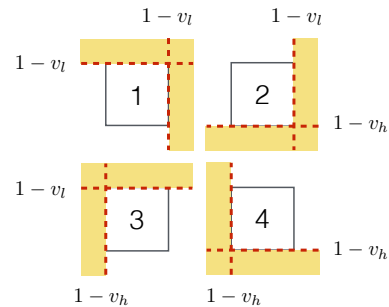


Figure 7: The stable points of both D-D and D-R coupled oscillator system should lie in the yellow shaded region for the system to oscillate. The system undergoes a transition to another state when the system hits the red dashed lines

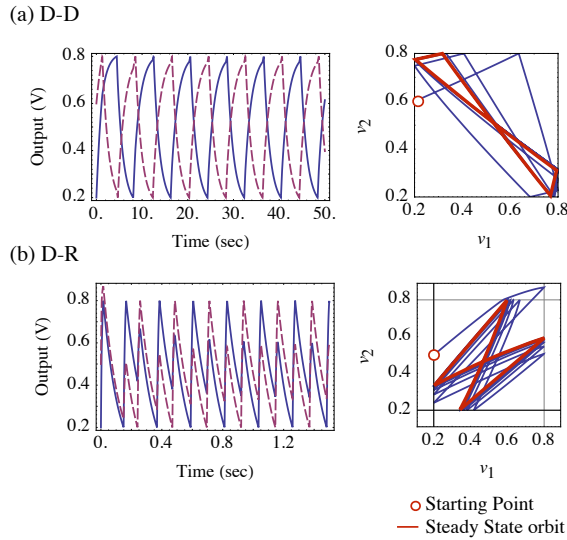


Figure 8: Simulation waveforms with time (left) and the system trajectory in phase space (right) of a system of coupled oscillators of type (a) D-D and (b) D-R. The steady state periodic orbit is shown in red. The butterfly shaped steady state trajectory corresponds to waveforms similar to anti-phase locking. The solid and dashed lines represent the two oscillators.

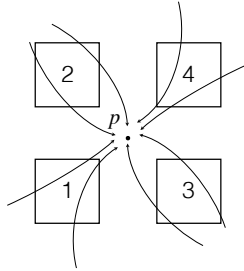


Figure 9: Combined phase space showing 4 regions of operation of the four different conduction states such that all states share a single fixed point p . This is possible as the flow matrices in all the four states are equal and, hence, all state spaces can be represented in a single space with a single flow but occupying different regions

ror image of itself about the eigen directions) as shown in figure 10. The stable fixed points in the conduction states 1(00), 2(01), 3(10) and 4(11) are $p_1 = (1, 1)$, $p_2 = \left(1 - \frac{1}{2+\beta}, \frac{1}{2+\beta}\right)$, $p_3 = \left(\frac{1}{2+\beta}, 1 - \frac{1}{2+\beta}\right)$ and $p_4 = (0, 0)$ respectively. Hence, the line along the eigen vector e_1 is the diagonal for both conduction states 1 and 4. Under the assumption that the v_{dd} normalized thresholds v_l and v_h are symmetric i.e. $v_l = 1 - v_h$, the line along e_2 also becomes the diagonal for states 2 and 3. This is because the fixed points of conduction states 2 and 3 - p_2 and p_3 lie on $x + y = 1$ line in their original state spaces which is same as the eigen direction e_2 . It should now be noted that the transitions between the conduction states, the regions of operation and the flow, all have the same common discrete symmetry - mirroring about e_1 and e_2 . We can do a symmetry reduction at this point and the system can be completely described by just two states and two transitions (figure 11a).

To study the steady state periodic orbits of this system, we calculate the return map on the left edge of state 1 in figure 11a which is $f = f_1 \circ f_2$. In this case, any periodic orbit in the sym-

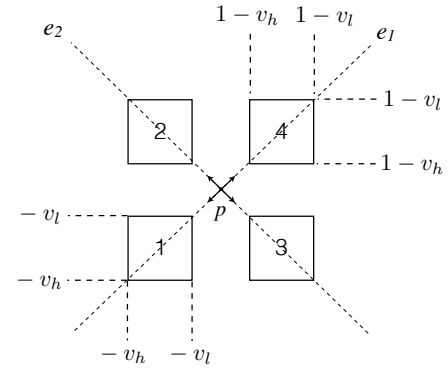


Figure 10: In the combined phase space, the flow of the coupled system is a mirror image of itself about its eigen vector directions e_1 and e_2 as the eigen values are real and negative. This symmetry of the flows can be reduced and the state space of the system can be described by considering just one-fourth of this space as shown in figure 11

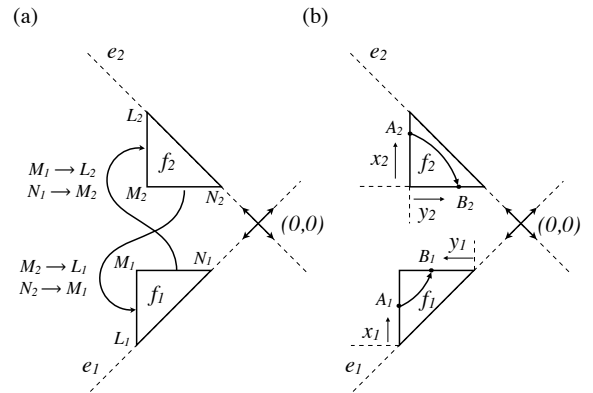


Figure 11: (a) Symmetry reduced space (fundamental domain) of the coupled system after reducing the symmetries shown in figure 10. f_1 is the mapping from the left edge of state 1 to its top edge and f_2 is the mapping from left edge of state 2 to its bottom edge. (b) Definition of x_1, x_2, y_1 and y_2 on the edges of the states in the symmetry reduced space

metry reduced space will correspond to at least one periodic orbit in the complete space (see figure 13). Also, if no fixed point exist in the symmetry reduced space, then there is definitely no periodic orbit in the complete space. The coordinate measurements on the edges are defined as shown in figure 11b. $f_1 : x_1 \rightarrow y_1$ is the mapping from the left edge of state 1 to its top edge and $f_2 : x_2 \rightarrow y_2$ is the mapping from left edge of state 2 to its bottom edge. x_1, x_2, x_3 and x_4 are defined on their respective edges as shown in figure 11b. As both the eigen values λ_1 and λ_2 are real and negative, $f_1(x)$ will lie above $x = y$ line and $f_2(x)$ will lie below it. A representative plot of f_1, f_2 and $f = f_1 \circ f_2$ (i.e. the return map $f : x_1 \rightarrow y_2$) is shown in figure 12 where $dv = v_h - v_l$. The composition $f = f_1 \circ f_2$ lies above $x = y$ if f_2 is more curved than f_1 and vice versa. As the return map is always increasing, only the first return map needs to be considered for finding fixed points and the higher return maps don't add new fixed points. When the coupling is more capacitive, the composition function tends to be concave as shown in figure 12a. Proposition 1 gives a mathematical form to this notion.

If the system moves from any arbitrary point on the flow,

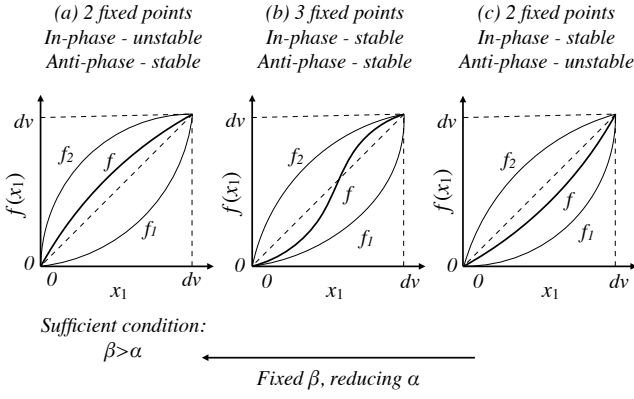


Figure 12: Representative plot of mappings f_1 , f_2 and their composition $f = f_1 \circ f_2$ with fixed β and varying α . Here $dv = v_h - v_l$. $\beta > \alpha$ is a sufficient condition for a concave f and hence stable anti-phase locking. As α increases, the curve for f transitions into a s-shaped curve with both in-phase and anti-phase lockings stable, and then finally to a convex curve with stable in-phase locking

say (x_a, y_a) to another point, (x_b, y_b) in time t then the following implicit equation can be written:

$$\left(\frac{x_a + y_a}{x_b + y_b} \right)^{\frac{1}{\lambda_1}} = \left(\frac{x_a - y_a}{x_b - y_b} \right)^{\frac{1}{\lambda_2}} \quad (21)$$

In state 1, (x_a, y_a) lies on the left edge and (x_b, y_b) lies on the top edge. To define $f_1 : x_1 \rightarrow y_1$ we substitute $(x_a, y_a) = (-v_h, -v_h + x_1)$ in equation (21) and obtain an implicit equation for f_1 as:

$$\left(\frac{2v_h - x_1}{2v_l + y_1} \right) = \left(\frac{x_1}{y_1} \right)^{\frac{\alpha+2}{\beta+2} \frac{\beta}{\alpha}} \quad (22)$$

Similarly, an implicit equation for $f_2 : x_2 \rightarrow y_2$ can be written as:

$$\left(\frac{k_\beta + x_2}{k_\beta - y_2} \right) = \left(\frac{dv - x_2}{dv - y_2} \right)^{\frac{\beta+2}{\alpha+2} \frac{\alpha}{\beta}} \quad (23)$$

where $k_\beta = \frac{\beta}{\beta+2}$.

Equations 22 and 23 can be solved numerically to obtain the steady state orbits of the system.

Proposition 1 : Sufficient condition for out-of-phase locking: For $\beta > \alpha > \frac{2dv}{1-dv} = \frac{dv}{v_l}$, i.e., $\frac{g_{dm}}{g_c} > \frac{c}{c_c} > \frac{2dv}{1-dv} = \frac{dv}{v_l}$ the coupled symmetric and identical system has only two steady state locking orbits - in-phase and out-of-phase. Further, the in-phase locking is unstable and the out-of-phase locking is stable.

Proof : The proof can be divided in two steps - (a) There are only two fixed points of f - at 0 and at dv , and (b) $f'(0) > 1$ and $f'(dv) < 1$ which implies that the in-phase locking is unstable and anti-phase locking is stable.

The first part is proved as follows.

As λ_1 and λ_2 are negative, $x_1 > y_1$ and $dv - x_2 > dv - y_2$. And as $\beta > \alpha > \frac{2dv}{1-dv}$, $\frac{\alpha+2}{\beta+2} \frac{\beta}{\alpha} > 1$ and $\frac{\beta+2}{\alpha+2} \frac{\alpha}{\beta} < 1$. Also $\beta > \frac{2dv}{1-dv}$ implies $k_\beta > dv > y_2$. This gives us the following

inequalities:

$$\left(\frac{2v_h - x_1}{2v_l + y_1} \right) \geq \left(\frac{x_1}{y_1} \right) \quad (24)$$

$$\text{and} \left(\frac{k_\beta + x_2}{k_\beta - y_2} \right) \leq \left(\frac{dv - x_2}{dv - y_2} \right) \quad (25)$$

where the equality holds at the end points i.e. at $x_1 = 0$ and $x_1 = dv$ for (24) and at $x_2 = 0$ and $x_2 = dv$ for (25). At any fixed point for the return map f , $x_1 = y_2$ and $y_1 = x_2$ and equations (24) and (25) should be consistent with these fixed point equations. Substituting $x_1 = y_2$ and $y_1 = x_2$ in (24) and (25) we get:

$$dv - ((dv - y_1) + y_2) + \frac{2(dv - y_1)y_2}{dv + k_\beta} \geq 0 \quad (26)$$

$$dv - ((dv - y_1) + y_2) + \frac{(dv - y_1)y_2}{v_h} \leq 0 \quad (27)$$

These equations are consistent only when

$$(dv - y_1)y_2 \frac{2}{dv + k_\beta} \geq (dv - y_1)y_2 \frac{1}{v_h} \quad (28)$$

which in turn can be true only at the end points, i.e. $y_1 = 0$ or $y_1 = dv$, because $k_\beta < 1$. It can be confirmed that this is indeed the case by inspection of figure 11.

The second part of the proof is proved by calculating $f'(0) = f'_1(0) \cdot f'_2(0)$. $f'_1(0)$ and $f'_2(0)$ are calculated from (22) and (23) as:

$$f'_1(0) = \left(\frac{v_l}{v_h} \right)^q \quad (29)$$

$$f'_2(0) = \frac{k_\alpha + dv}{k_\alpha - dv} = \frac{k_\alpha + v_h - v_l}{k_\alpha - v_h + v_l} > \frac{v_h}{v_l} \quad (30)$$

where $q = \frac{\beta+2}{\alpha+2} \frac{\alpha}{\beta} < 1$ and $k_\alpha = \frac{\alpha}{\alpha+2}$. Also $\alpha > \frac{2dv}{1-dv}$ implies $k_\alpha > dv$. Hence

$$f'(0) = f'_1(0) \cdot f'_2(0) > \left(\frac{v_h}{v_l} \right)^{1-q} > 1 \quad (31)$$

And as f has no other fixed points between 0 and dv and f is continuous, $f'(dv) < 1$. Hence, proved.

It should be noted that this condition is not a strict bound but rather provides key design insights when a particular form of coupling (anti-phase) is sought¹.

A. Capacitive, Resistive Coupling and Bistable Orbits

The two extreme cases of purely resistive and purely capacitive coupling are of interest. In case of coupling using only a capacitor, the symmetric and identical coupled system always has a stable anti-phase and an unstable in-phase locking. This is because in case of purely capacitive coupling, $\beta \rightarrow \infty$ and so $\beta > \alpha$ for all finite α . Even in practical cases where some parasitic resistance is included in parallel with the coupling capacitor², β is typically much larger than α . Such anti-phase locking matches well with recent experimental findings of capacitively MIT coupled oscillators as discussed in¹. In case of coupling using only a resistor, the symmetric and identical coupled system will have a stable in-phase and an unstable anti-phase orbit, as can be predicted from figure 15 for

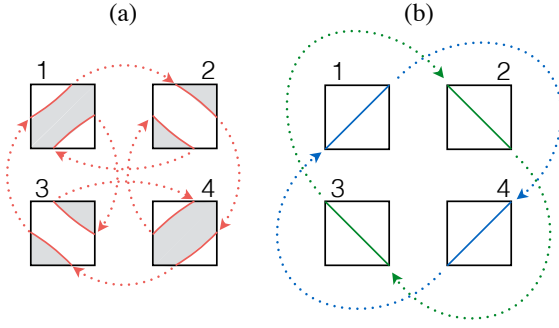


Figure 13: The trajectories (which are periodic orbits) corresponding to the fixed points in the return maps of figure 12b. (a) The unstable fixed point of figure 12b corresponds to two periodic orbits in the unreduced space as shown in red. (b) The fixed point at 0 corresponds to a single periodic orbit shown in blue and the fixed point at dv corresponds to the green periodic orbit. When the initial state of the system lies in the gray region (shown in (a)), the system settles down to an in-phase locking state, and otherwise to an anti-phase locking state

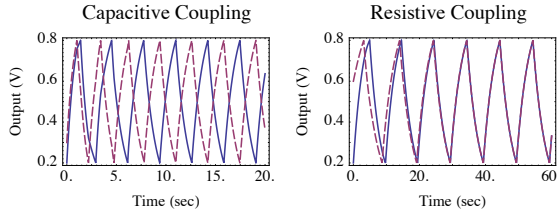


Figure 14: Capacitive coupling leads to anti-phase locking and resistive coupling leads to in-phase locking in case of symmetric D-D coupled. The solid and dashed lines represent the two oscillators.

$\alpha \rightarrow \infty$. Time domain simulations of the coupled systems with purely capacitive and purely resistive coupling are shown in figure 14. The parameter values for capacitive coupling are $\alpha = 5$ and $g_{dm} = g_s = 6c_c$ and those for resistive coupling are $c = 13g_c$ and $\beta = 3.6$.

Figure 12 (b and c) show cases when $\beta < \alpha$. In the intermediate case when the return map transitions from concave to convex, the system goes through a state where both in-phase and anti-phase locking are stable with one unstable fixed point in between (figure 12b). In figure 15 the two regions for concave and convex return map can be clearly seen. They are separated by a thin region which represents the case of bistability. Figure 16 shows the time domain simulation waveforms of oscillator outputs for $\beta = 3.6$ and $\alpha = 13.1$. We note that the initial voltage of the first oscillator is 0.2V and depending on the initial voltage of the second oscillator, the system can either lock in phase or out of phase. These design parameters correspond to a bistable system of the kind shown in figure 12b, and hence the final steady state locking is in-phase or out-of-phase depending on the initial phase of the system. When the initial phase (or output voltage) of oscillators are close to each other (represented by gray region in figure 13a) the system locks in-phase, and when they are far the system locks out-of-phase for the same circuit parameters.

VI. Asymmetric D-D coupled oscillator dynamics

Let us now investigate the case of D-D oscillator dynamics where the two oscillators are identical but the pull-up and pull-

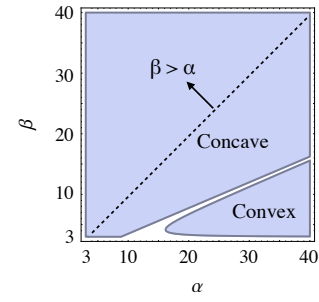


Figure 15: Return map type for the symmetric D-D case in the parametric space, $\beta \times \alpha$ for $v_l = 0.2$ and $v_h = 0.8$. We can clearly see that for $\beta > \alpha$ the return map is concave and anti-phase locking is stable. Also when the coupling is more resistive, the return map becomes convex with stable in-phase locking. The region between concave and convex return map is the region with S-shaped return map with both stable in-phase and stable anti-phase locking

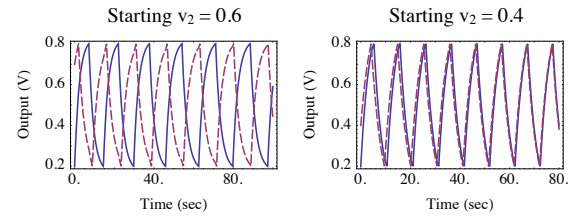


Figure 16: Simulation waveforms showing the dependence of final locking to the initial state of the system in the intermediate case of figure 12b when the return map is S-shaped. The solid and dashed lines represent the two oscillators. Initial $v_1 = 0.2V$ in both cases, but the system locks in-phase when initial $v_2 = 0.4V$, and anti-phase when initial $v_2 = 0.6V$. With reference to figure 13, the initial point $(0.2, 0.4)$ lies in the gray region and the point $(0.2, 0.6)$ lies outside the gray region in conduction state 1

down devices are non-identical thereby giving rise to asymmetric charging and discharging rates. As the the oscillators are identical, $\beta_{11} = \beta_{21} = \beta_c$ and $\beta_{12} = \beta_{22} = \beta_d$ where subscripts c and d stand for charging and discharging. The symmetry of the system (due to the identical oscillators) can be seen in the flows of the states. Flows of conduction states 1(00) and 4(11) are mirror images about the diagonal $x = y$ and the flow in conduction state 2(10) is equivalent to the flow in state 3(01) with axes x and y interchanged. This symmetry is also shown in the transitions between states. The system can be expressed after reducing the symmetry as in figure 17. For $\beta_c < \beta_d$, two kinds of cycles are possible in the regions $1 \rightarrow 2b \rightarrow 1$ and $1 \rightarrow 2c \rightarrow 4 \rightarrow 2a \rightarrow 1$. To find the fixed points of the system, we draw the return map with the bottom edge of state 1 as the Poincare section. Because it is a symmetry reduced space, we consider the first return map for trajectories of the type $1 \rightarrow 2c \rightarrow 4 \rightarrow 2a \rightarrow 1$ and the second return map for trajectories of the type $1 \rightarrow 2b \rightarrow 1$. Let $f_1(x'_k) = x_k$ as shown in figure 18 where f_1 is the mapping from bottom edge of conduction state 1 to its right edge, and f_{2a}, f_{2b} and f_{2c} are the mappings between edges in conduction state 2 as shown. Then the return map f is given by:

$$f(x) = \begin{cases} f_1 \circ f_{2c} \circ f_4 \circ f_{2a}(x), & 0 \leq x < x'_k \\ f_1 \circ f_{2b} \circ f_1 \circ f_{2b}(x), & x'_k \leq x < dv \end{cases} \quad (32)$$

Proposition 2 : Existence of stable periodic orbit in asymmet-

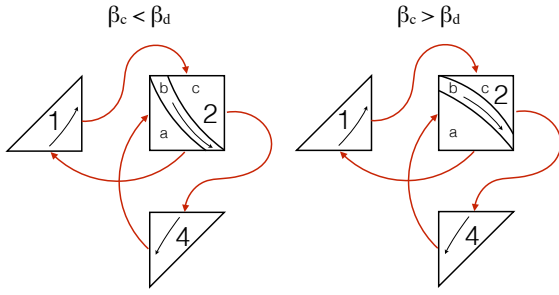


Figure 17: Symmetry reduced space in the asymmetric D-D configuration with $\beta_c > \beta_d$ (left) and $\beta_c < \beta_d$ (right). Such configuration will have only a single symmetry. The flow matrices in the four conduction states are not equal and hence states cannot be represented in a single combined state space with a single fixed point as was done in the symmetric D-D case ($\beta_c = \beta_d$)

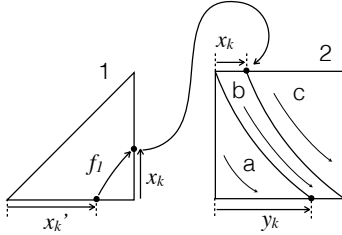


Figure 18: Diagram of symmetry reduced state spaces for conduction states 1 and 2 in the asymmetric D-D configuration. In conduction state 2, the top-left corner does not map to the bottom-right corner as was the case in the symmetric D-D case. The width of this middle region where the flow maps the top edge to the bottom edge is defined using x_k and y_k

ric D-D coupled oscillator system: If f is the return map for the D-D asymmetric coupled oscillator on the bottom edge of state 1 then the following are true:

- f is continuous
- $f'(0) > 1$ for $\beta_c > \alpha$ and $\beta_d > \alpha$
- f has one fixed point at 0 and at least one in the interval $x'_k < x < dv$ at, say, x_f
- Either the fixed point at x_f is stable, or there exists a stable fixed point at x'_f where $0 \leq x'_f < x_f$

Proof : (a) The return map is separately continuous in intervals $[0, x'_k]$ and $(x'_k, dv]$ as it is a composition of mappings of continuous flows. The continuity of f at x_k can be established by considering two points close to x'_k on either side. From (32) we can see that $f(x'_{k+}) = f(x'_{k-}) = y_k$, and hence f is continuous at x_k .

(b) It can be proved by similar procedure as adopted before in *Proposition 1* that $f'(0) = f'_1(0) \cdot f'_{2c}(dv) \cdot f_4(0) \cdot f'_{2a}(0) > 1$ for $\beta_c > \alpha$ and $\beta_d > \alpha$.

(c) The fixed point at 0 can be seen clearly in the flow diagram. In interval $x'_k < x < dv$, the fixed points of first return $f_1 \circ f_{2b}$ will also be the fixed points of second return (which is f), but not the other way around. Now $f_1 \circ f_{2b}(x'_k) = dv$ and $f_1 \circ f_{2b}(dv) = y_k$. As $f_1 \circ f_{2b}$ is continuous, and hence decreasing, in the interval $x'_k < x < dv$, there exists a fixed point for $f_1 \circ f_{2b}$, and hence for f , in the interval $x'_k < x < dv$.

(d) As f is continuous and has fixed points at 0 and x_f , one of these two should be stable if there is no other fixed point in between 0 and x_f . If they both are unstable, then

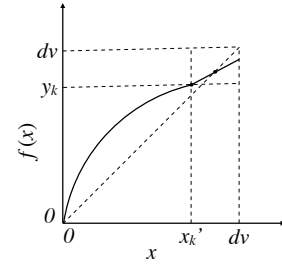


Figure 19: Representative plot of the return map on the bottom edge of conduction state 1 in the asymmetric D-D case. The fixed point corresponding to anti-phase locking which was at dv in the symmetric case is shifted inside away from dv in the asymmetric case

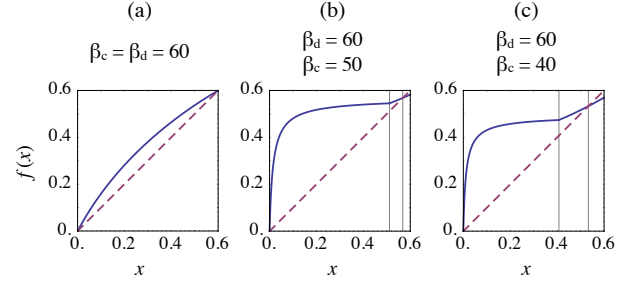


Figure 20: Comparison of return maps in the symmetric (a) and asymmetric (b and c) D-D configurations for constant $\alpha = 10$. Both symmetric and asymmetric configurations have a fixed point at 0 corresponding to in-phase locking (which is unstable here as $\beta > \alpha$ condition is satisfied) along with another fixed point, which in symmetric case, is at dv (perfect anti-phase locking) but in asymmetric case shifts away from dv

a stable fixed point exists in the interval $(0, x_f)$. Hence proved.

Figure 19 shows a representative return map for the asymmetric D-D configuration. The poincare section chosen in the symmetric D-D case was the left edge of conduction state 1. Due to symmetry, the left edge of conduction state 1 is same as the bottom edge of conduction state 1. Hence the return maps in the symmetric D-D case can be compared with the return maps in the asymmetric D-D case as if they were drawn on the same edge. Figure 20 shows a comparison of the return maps of a symmetric case ($\beta_c = \beta_d = 60, \alpha = 10$) with that of two asymmetric cases ($\beta_c = 50$ and $40, \beta_d = 60, \alpha = 10$). The corresponding time domain waveforms and phase plots are shown in figure 20. The figure clearly shows that the steady state periodic orbit changes from a diagonal (perfect anti-phase locking) to a butterfly shaped curve (imperfect anti-phase locking) as the asymmetry increases. However, the time domain waveforms for butterfly shaped periodic orbits would still be very similar in appearance to anti-phase locking. The fixed point close to dv in the return map shifts away from dv as the difference between β_c and β_d increases. This trend can be seen in figure 22 which shows the movement of the anti-phase fixed point with $\beta_d - \beta_c$ for fixed $\beta_d = 60$ and $\alpha = 10$. For $\beta_c > \beta_d$, the cycles will be of the type $4 \rightarrow 2b \rightarrow 4$ and $1 \rightarrow 2c \rightarrow 4 \rightarrow 2a \rightarrow 1$, and the return map will have to be drawn on an edge of state 4. The return map in this case will be analogous to the $\beta_c < \beta_d$ case with β_c and β_d interchanged.

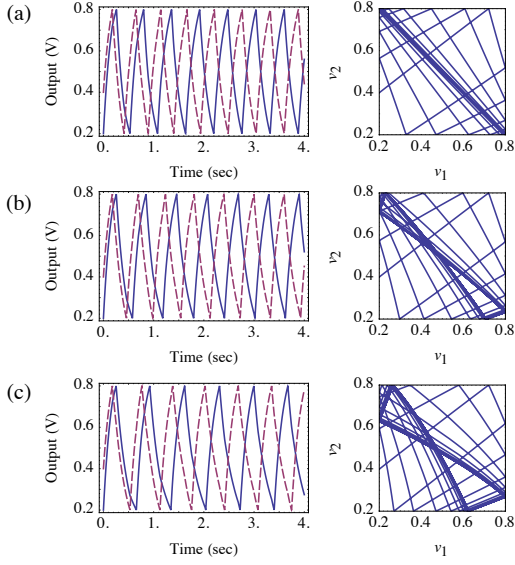


Figure 21: Time domain waveforms and phase plots corresponding to the configurations in figure 20(a, b and c). The steady state periodic orbits can be seen clearly in the phase plots to transform from a diagonal (perfect anti-phase locking) in the symmetric case (a) to a butterfly shaped curve (imperfect anti-phase locking) as the asymmetry increases and the anti-phase fixed point in the return map shifts away from dv

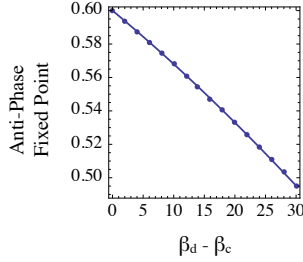


Figure 22: Numerical simulations illustrating the fixed point close to dv shifts away from dv with increasing difference between β_c and β_d in the asymmetric case

VII. D-R coupled oscillator dynamics

In this section we consider the dynamics of a D-R coupled system. This is of interest because of its ease of fabrication, relaxed conditions for oscillations and already published reports of such coupled oscillatory systems². We consider coupling of identical oscillators and hence we define $\beta_1 = \beta_2 = \beta$ and $\beta_{s1} = \beta_{s2} = \beta_s$. Unlike the D-D coupled oscillator case, the notion of symmetric charging and discharging does not apply in D-R coupled oscillator case because the circuit by construction is different for charging and discharging. During charging a part of the net charging current charges up the output capacitor whereas the rest of it flows through the pull-down resistance to ground. The process of discharging has no such leakage component. In terms of the conductance ratio β , this can be explained by the fact that the net charging component in the matrix A is $(\beta + \beta_s)$ and it is always greater than the discharging component β_s . However, the flows can still be simplified for analysis as was described in section IV. The simplification assumes that the flows are monotonic in the regions of operation in all four conduction states, but the

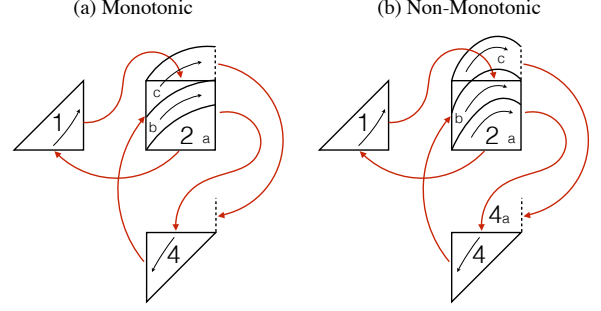


Figure 23: Symmetry reduced space in the D-R coupled oscillator system. There is only a single symmetry due to identical oscillators

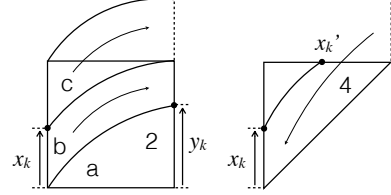


Figure 24: Symmetry reduced space for the D-R coupled oscillator system in states 1 and 4 with the definition of x_k , x_k' and y_k . f_4 is the mapping from top edge of state 4 to left edge of state 4 and f_{2a} , f_{2b} and f_{2c} are mappings between edges of state 2 as shown

direction of monotonicity is different from the D-D coupled oscillator case as shown in figure 6. For our analysis, a particular type of non-monotonicity is allowed in state 2 (and state 3) as shown in figure 23. Here the fixed point for conduction state 2 satisfies the condition of oscillation shown in figure 7, but the flow in state 2 as shown in the symmetry reduced space (figure 23) is non monotonic. We will consider the case of identical oscillators, and following the methodology of the asymmetric D-D case, we can reduce the symmetry of identical oscillators as shown in figure 23. In this case, two kinds of cycles are possible - $4 \rightarrow 2b \rightarrow 4$ and $4 \rightarrow 2c \rightarrow 4a \rightarrow 4$. To find the fixed points of the system, we draw the return map on the top edge of conduction state 4 as the Poincare section. Because it is a symmetry reduced space, we will have to consider the second return map for cycles of the type $4 \rightarrow 2b \rightarrow 4$ but only the first return map for $4 \rightarrow 2c \rightarrow 4a \rightarrow 4$ type cycles. Let f_4 be the mapping from top edge of state 4 to its left edge, f_{4a} be the mapping from the extended right edge of state 4 to its top edge, f_{2a} , f_{2b} and f_{2c} be the mappings between edges of state 2, and $f_4(x_k') = x_k$ as shown in figure 24. Then the return map f is given by:

$$f(x) = \begin{cases} f_4 \circ f_{2c} \circ f_{4a}(x), & 0 \leq x < x_k' \\ f_4 \circ f_{2b} \circ f_4 \circ f_{2b}(x), & x_k' \leq x < dv \end{cases} \quad (33)$$

Proposition 3: Conditions for existence of stable periodic orbit in D-R coupled oscillator system: If f is the return map for the D-R coupled oscillator system on the top edge of state 4 in the symmetry reduced state space (figure 23) then

- f is piece-wise continuous with discontinuity at x_k' . Moreover, $f(x_k'_{+}) = y_k$ and $f(x_k'_{-}) = dv$.
- f has at least one fixed point in the interval $x_k' < x < dv$ at, say, x_f
- If $y_k > x_k'$, f has at least one stable fixed point in the

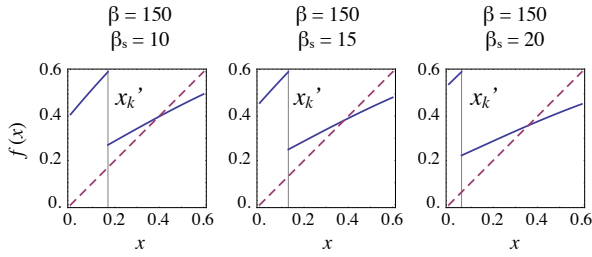


Figure 25: Return map on the top edge of state 4 for the D-R coupled oscillator system for $\alpha = 1$, $\beta = 150$ and β_s values of 5, 10 and 20

interval $x'_k < x < dv$

Proof : (a) The argument is the same as in *Proposition 2*. The return map is separately continuous in intervals $[0, x'_k)$ and $(x'_k, dv]$ as it is the composition of continuous flows. From (33) we can see that $f(x'_{k+}) = y_k$ and $f(x'_{k-}) = dv$.

(b) In the interval $x'_k < x < dv$, the fixed points of the first return map $f_4 \circ f_{2b}$ will also be the fixed points for its second return map (which is f). Now $f_4 \circ f_{2b}(x'_k) = dv$ and $f_4 \circ f_{2b}(dv) = y_k$. As $f_4 \circ f_{2b}$ is continuous (and hence decreasing) in this interval, there exists a fixed point for $f_4 \circ f_{2b}$, and hence f , in the interval $x'_k < x < dv$.

(c) As $f(x'_{k+}) = y_k$, f is continuous in the interval $x'_k < x < dv$ and f has a fixed point at x_f where $x'_k < x_f < dv$, hence either the fixed point at x_f is stable or there exists another fixed point in the interval $x'_k < x < x_k$ which lies in $x'_k < x < dv$. Hence proved.

Figure 25 shows the return map f on the top edge of state 4 for the D-R coupled oscillator system for varying β_s . The return maps in the figure have a single stable fixed point at x_f in the interval $x'_k < x < dv$. The movement of the fixed point x_f with β_s is shown in figure 26.

Another important design consideration for the coupled oscillator system, is the role of the coupling circuit on the overall system dynamics, as is seen in figure 27. We note that as the value of α increases the phase diagram in the $v_1 \times v_2$ plane shows strong sensitivity. In particular, for low values of α , the system shows in-phase locking. As α increases (for intermediate value of α), the butterfly shaped phase plot widens and the system exhibits a non-monotonic decrease in the output voltages, v_1 and v_2 from v_h to v_l . This can also be seen in the time domain waveforms where the output voltages first decrease to an intermediate voltage, then increase and again decrease; clearly demonstrating four possible conduction states (MM, MI, IM and II) in both phase and time domain plots. Finally, for high values of α the butterfly in the phase plot opens even further, thus making the decrease of output voltages from v_h to v_l more monotonic and the system tends to anti-phase locking, as exhibited in both phase and time (figure 27).

VIII. Experimental verification

An MIT device can be realized using VO_2 (Vanadium dioxide) which exhibits unique electronic properties like metal-insulator phase transitions. VO_2 has been shown to undergo abrupt first order metal-to-insulator and insulator-to-metal transitions with upto five orders of change in conductivity¹⁸

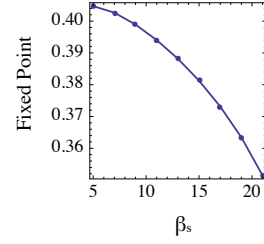


Figure 26: Movement of the fixed point x_f for fixed $\alpha = 1$, $\beta = 150$ and varying β_s for the return map on the top edge of state 4 for the D-R coupled oscillator system

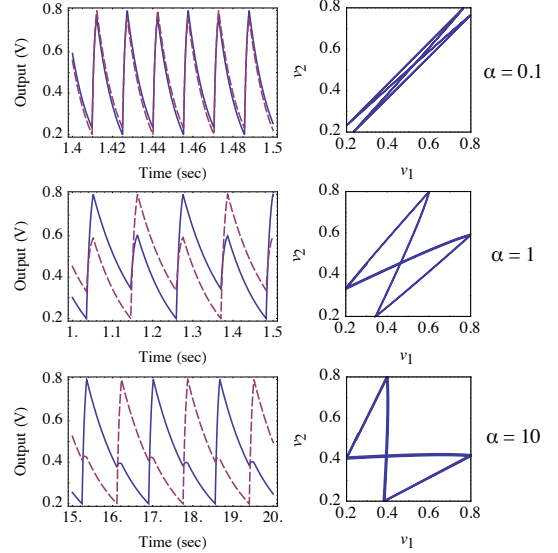


Figure 27: Steady state waveforms and phase trajectories for the D-R coupled oscillator system with $\alpha = 0.1$ (top), $\alpha = 1$ (middle) and $\alpha = 10$ (bottom). The solid and dashed lines represent the two oscillators.

and ultra-fast switching times¹⁶. Transitions have been shown to be electrically driven, thermally driven or a combination thereof. Recent work shows that for such a transition, a metallic filament structure is formed which acts as a conduction pathway in the low resistance state of VO_2 ¹⁹. Also, a series circuit of VO_2 with a resistive pull down network has been shown to exhibit self-sustained electrical oscillations² when conditions of oscillations as described above are met. Moreover, two such relaxation oscillators can be electrically coupled to produce synchronized oscillations².

For experimental validation, we apply our models of coupled relaxation oscillators on a system of two coupled VO_2 oscillators. Figure 28 shows a schematic representation of the coupled circuit with a parallel resistance (R_C) and capacitance (C_C) as the coupling circuit. Frequency domain results of this system have been previously reported² showing a close match between experiments and theoretical results of a D-D model; and are not reproduced here. Using the D-R model developed in this paper, we obtain close match in the time-domain and phase plots of the oscillator system as well. With proper calibration of the system parameters, the D-R model described above shows very close qualitative match with experimental results. One such experimental result has been shown in figure 29 along with model prediction. This validation of the pro-

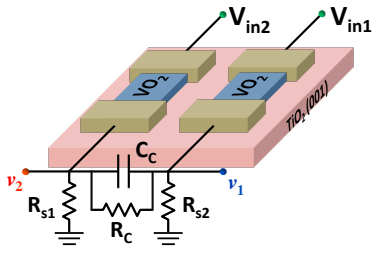


Figure 28: Schematic of the experimental setup of coupled VO_2 oscillators, with series resistances R_{s1} and R_{s2} respectively, coupled using a parallel $R_C - C_C$ circuit

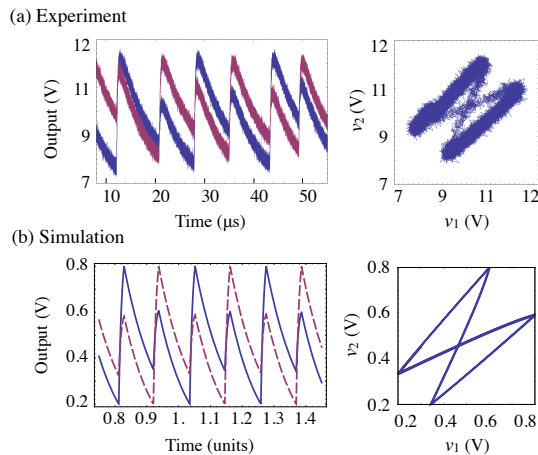


Figure 29: Experimental and simulated time domain waveforms in the steady state and phase plots for a parallel $R_C - C_C$ coupled oscillator system. The D-R coupled relaxation oscillator model is used for model development and simulation. The two waveforms show close match and validate the model prediction.

posed models enables further design of experiments. It further models and explains both qualitative and quantitative the role of the system design parameters on the rich synchronization dynamics.

IX. Conclusions

This paper presents a model study of the synchronization dynamics of a pair of identical and electrically coupled relaxation oscillators when physically realized using MIT devices. Experimental realization of such devices^{1,2} has motivated the study of their dynamics, with emphasis on phase synchronization, locking conditions and potential programmability of the phase relations using electrical means. We investigate the case of a purely MIT based oscillator (D-D) and that of a hybrid oscillator composed of an MIT device and a passive resistance (D-R configuration). We show through numerical and analytical techniques, validated against experimental results, the existence of out-of-phase locking (in purely capacitive coupling), in-phase locking (in purely resistive circuits) and the possibility of bistable circuits (for intermediate values of R and C). This opens new paradigms for realizing associative computing networks using coupled oscillators by enabling model studies of such physically realizable circuit elements.

Acknowledgments

NS and SD acknowledge funding from the Office of Naval Research through award N00014-11-1-0665. SD would also like to acknowledge funding, in part, from the NSF Expeditions in Computing Award-1317560. AP and AR would like to acknowledge the generous gift of Intel Corporation which made this work possible.

References

- Suman Datta, Nikhil Shukla, Matthew Cotter, Abhinav Parihar, and Arijit Raychowdhury. Neuro inspired computing with coupled relaxation oscillators. In *Proceedings of the The 51st Annual Design Automation Conference on Design Automation Conference*, pages 1–6. ACM, 2014.
- Nikhil Shukla, Abhinav Parihar, Eugene Freeman, Hanjong Paik, Greg Stone, Vijaykrishnan Narayanan, Haidan Wen, Zhonghou Cai, Venkatraman Gopalan, Roman Engel-Herbert, et al. Synchronized charge oscillations in correlated electron systems. *Scientific reports*, 4, 2014.
- Florian Dörfler and Francesco Bullo. Exploring synchronization in complex oscillator networks. *arXiv preprint arXiv:1209.1335*, 2012.
- Arthur T Winfree. Biological rhythms and the behavior of populations of coupled oscillators. *Journal of theoretical biology*, 16(1):15–42, 1967.
- Yoshiki Kuramoto. Self-entrainment of a population of coupled non-linear oscillators. In *International symposium on mathematical problems in theoretical physics*, pages 420–422. Springer, 1975.
- Yoshiki Kuramoto. *Chemical oscillations, waves, and turbulence*. Courier Dover Publications, 2003.
- Dmitri E Nikonov, Gyorgy Csaba, Wolfgang Porod, Tadashi Shibata, Danny Voils, Dan Hammerstrom, Ian A Young, and George I Bourianoff. Coupled-oscillator associative memory array operation. *arXiv preprint arXiv:1304.6125*, 2013.
- Eugene M Izhikevich. Computing with oscillators. 2000.
- Enrique Mallada and Ao Tang. Synchronization of weakly coupled oscillators: coupling, delay and topology. *Journal of Physics A: Mathematical and Theoretical*, 46(50):505101, 2013.
- Juan A Acebrón, Luis L Bonilla, Conrad J Pérez Vicente, Félix Ritort, and Renato Spigler. The kuramoto model: A simple paradigm for synchronization phenomena. *Reviews of modern physics*, 77(1):137, 2005.
- RH Rand and PJ Holmes. Bifurcation of periodic motions in two weakly coupled van der pol oscillators. *International Journal of Non-Linear Mechanics*, 15(4):387–399, 1980.
- DW Storti and RH Rand. Dynamics of two strongly coupled van der pol oscillators. *International Journal of Non-Linear Mechanics*, 17(3):143–152, 1982.
- A Kouda and S Mori. Mode analysis of a system of mutually coupled van der pol oscillators with coupling delay. *International Journal of Non-Linear Mechanics*, 17(4):267–276, 1982.
- Tapesh Chakraborty and Richard H Rand. The transition from phase locking to drift in a system of two weakly coupled van der pol oscillators. *International Journal of Non-Linear Mechanics*, 23(5):369–376, 1988.
- T. Saito. On a coupled relaxation oscillator. *Circuits and Systems, IEEE Transactions on*, 35(9):1147–1155, Sep 1988.
- Ayan Kar, Nikhil Shukla, Eugene Freeman, Hanjong Paik, Huichu Liu, Roman Engel-Herbert, S. S. N. Bharadwaja, Darrell G. Schlom, and Suman Datta. Intrinsic electronic switching time in ultrathin epitaxial vanadium dioxide thin film. *Applied Physics Letters*, 102(7):–, 2013.
- Chia-Lun Hu. Self-sustained oscillation in an $R_H - C$ or $R_H - L$ circuit containing a hysteresis resistor r_H . *Circuits and Systems, IEEE Transactions on*, 33(6):636–641, Jun 1986.
- Larry A. Ladd and William Paul. Optical and transport properties of high quality crystals of $\{V_2O_4\}$ near the metallic transition temperature. *Solid State Communications*, 7(4):425 – 428, 1969.
- Eugene Freeman, Greg Stone, Nikhil Shukla, Hanjong Paik, Jarrett A Moyer, Zhonghou Cai, Haidan Wen, Roman Engel-Herbert, Darrell G Schlom, Venkatraman Gopalan, et al. Nanoscale structural evolution of electrically driven insulator to metal transition in vanadium dioxide. *Applied Physics Letters*, 103(26):263109, 2013.